Supplementary Tables

Table S1. List of the oligos used for RT-PCR analysis

Oct4	Fw CGTGGAGACTTTGCAGCCTG	Rv GCTTGGCAAACTGTTCTAGCTCCT
Sox2	Fw GGCAGAGAAGAGAGTGTTTGC	Rv TCTTCTTTCTCCCAGCCCTA
Pax6	Fw CCACCCATGCCCAGCTT	Rv AACTGACACTCCAGGTGAAATGAG
Nestin	Fw TGGAAGTGGCTACA	Rv TCAGCTTGGGGTCAGG
Six3	Fw GTGGACGGCGACTCTGC	Rv CAACTGGTTTAAGAACCGGC
Chx10	Fw ATCCGCAGAGCGTCCACT	Rv CGGTCACTGGAGGAAACATC
Math3	Fw AGCTGACCCCGGGAAAGAGAATC	Rv AGCCCGGTCTTCTCTCTTGCT
Math5	Fw TGGGGCCAGGACAAGAAGCTGT	Rv ATGCGGGTGAGCGCGATGAT
Prox1	Fw TGAATCCCCAAGGTTCTGAG	Rv AAAGGCATCATGGCATCTTC
Ascl-1	Fw GTTGGTCAACCTGGGTTTTG	Rv CCTTGCTCATCTTCTTGTTGG
CyclinD1	Fw GAGATTGTGCCATCCATGC	Rv CTCCTCTTCGCACTTCTGCT
Gapdh	Fw GTATGACTCCACTCACGGCAAA	Rv TTCCCATTCTCGGCCTTG

Table S2. List of primary antibodies used for immunofluorescence staining

Antibody	Concentration	Provider
Rabbit anti-glutamine synthetase (GS)	1:300	Sigma G-2781
Mouse anti retinaldehyde-binding protein (CRALBP)	1:300	Abcam AB 15051
Mouse anti-proliferating cell nuclear antigen (PCNA)	1:200	Sigma P8825
Rabbit anti-phospho-histone H3 (pH3)	1:200	Millipore 06-570
Chicken anti-green fluorescent protein (GFP)	1:500	Abcam AB13970
Rabbit anti-recoverin (REC)	1:500	Millipore AB5585
Rabbit anti-calbindin D-28K (CALB)	1:100	Sigma C7354
Mouse anti-calretinin (CALR)	1:200	Millipore MAB1568
Mouse anti-Nestin	1:200	Abcam AB6142
Rabbit anti-protein kinase C (PKC)	1:200	Santa Cruz Biotechnology sc-208, Lot L2414
Rat anti-MAC-1	1:300	Abcam AB8878

Supplementary Figure Legends

Figure S1. Müller glial cells (MGCs) undergo de-differentiation and re-enter the cell cycle following NMDA-damage. (a) Graphical scheme illustrating how the retinal layers can be distinguished in flat mounts. Retinal layers are spatially organized, as shown in the 3D graphical representation (left panel). The different morphology and size of $DAPI^+$ nuclei allow discrimination among neuronal populations. For instance, nuclei of photoreceptors are of higher intensity and smaller than those of ganglion cells and interneurons. Confocal microscopy allows to image any desired layer at a time. Accordingly, in the right panel, we have provided images of a flat mount stained with layer-specific markers: rhodopsin for photoreceptors in the outer nuclear layer; glutamine synthase for MGCs of the inner nuclear layer; beta-III tubulin for ganglion neurons in the ganglion cell layer. (b) Representative images of retinal flat mount from undamaged GFAP-Cre/R26Y mice. Retinae were stained for YFP (green) and the MGC-specific marker CRALBP (red). Yellow arrows indicate co-localization of the YFP signal with CRALBP expression (MGCs). Red arrows indicate YFP^+ cells negative for CRALBP. Zoomed areas are included in the white boxes. Scale bar: 25 μm. (c) FACS plots showing YFP^+ cell populations sorted from control (CTR) and NMDA-damaged (24 hpi, 4 dpi) retinae of GFAP-Cre/R26Y lineage tracing mice. Dead cells were excluded by gating on $DAPI^-$ cells. (d) RT-PCR expression analysis of *Cyclin D1* using total RNAs harvested from YFP^+ cells FACS-sorted from PBS-treated (CTR) and NMDA-damaged (NMDA) retinae of GFAP-Cre/R26Y mice, 24hpi and 4dpi. Transcript levels are expressed as fold-changes relative to YFP^+ cells sorted from control retinae. Data are represented as mean ± S.E.M. (n = 4). Statistical analysis is based on unpaired Student's T-test (24 hpi, $p = 0.0474^*$; 4 dpi, $p = 0.0136^*$). (e) Confocal images of retinal sections from PBS-treated (CTR) and NMDA-damaged (NMDA) retinae of GFAP-Cre/R26Y mice, harvested 4dpi. Proliferative cells are immunopositive for PCNA (red, left panels) and pH3 (red, right panels). Yellow

arrows show proliferative YFP$^+$ cells in the inner nuclear layer (inl). Zoomed images of areas included in the white boxes are shown in the bottom-left corners. Nuclei were counter stained with DAPI (blue). Scale bar: 20 μm (n = 3). (f) Representative images from flat mounts of PBS-treated (CTR) and NMDA-damaged (NMDA) GFAP-Cre/R26Y mice, harvested 4dpi. Yellow arrows show proliferative YFP$^+$ cells. Zoomed images of areas included in the white boxes are shown in the top-right corners. (g) Representative field from a NMDA-damaged GFAP-Cre/R26Y mouse sacrificed 3 wpi. YFP$^+$ cells (green) differentiating into beta-III tubulin$^+$ cells (red,) are indicated by yellow arrows. Nuclei were counterstained with DAPI (blue) (n = 3).

Figure S2. The SDF1/CXCR4 signaling axis affects damage-dependent de-differentiation and proliferation of Müller glia cells. (a) RT-PCR analysis of SDF1 expression in YFP$^+$ cells FACS-sorted 24 hpi from PBS-treated (CTR) and NMDA-damaged (NMDA) retinae of GFAP-Cre/R26Y mice. Transcript levels are expressed as fold-changes relative to YFP$^+$ cells from CTR retinae. Values represent the mean ± S.E.M. (n = 3). Statistical analysis is based on unpaired Student's T-test (p = 0.3660^{ns}). (b) FACS plots showing YFP$^+$ cell populations sorted 4 dpi from the retinae of GFAP-Cre/R26Y lineage tracing mice of the four treatment groups (PBS, NMDA, NMDA + SDF1, NMDA + AMD3100). Dead cells were excluded by gating on DAPI$^-$ cells. (c) Amount of YFP$^+$ cells in GFAP-Cre/R26Y lineage tracing mice analyzed by FACS 4dpi, for the various treatment groups (NMDA n = 9, NMDA + SDF1 n = 6, NMDA + AMD3100 n = 6). Values are expressed as fold changes relative to the number of YFP$^+$ cells present in the PBS-injected controls. Statistical analysis is based on One-way Anova (p = 0.0124*) followed by Turkey's multiple comparisons test (significance indicated in the figure). (d) Representative immunostaining images of 4 dpi flat-mounted retinae from GFAP-Cre/R26Y lineage tracing mice belonging to the various treatment groups (NMDA, NMDA +

SDF1, NMDA + AMD3100). YFP^+ cells (green) also positive for Nestin (red) are indicated by yellow arrows. Images were chosen from random fields of stained flat mounts from 2 different eyes per treatment group (n = 2). Cell nuclei were counterstained with DAPI. Scale bar: 20 μm. (e) Percentage of $Nestin^+$ cells calculated over the total number of YFP^+ cells. Cells were counted in random fields of 4dpi retinal flat mounts harvested from GFAP-Cre/R26Y mice belonging to the various treatment groups (NMDA n = 7, NMDA + SDF1 n = 4, NMDA + AMD3100 n = 7). Statistical analysis is based on One-way Anova ($p = 0.0003^{***}$) followed by Turkey's multiple comparisons test (significance indicated in the figure).

Figure S3. Dedifferentiated YFP^+ cells are not apoptotic 3 weeks post-injury. (a) Representative images of PBS-injected (CTR) and NMDA-damaged (NMDA) retinal flat mounts from wild type mice. TUNEL staining was performed 1week post-injection (1 wpi, n = 2). Zoomed images of the areas included in the white boxes are shown in the upper-right corners. Scale bar: 50 μm. (b) Representative images of retinal flat mounts from PBS-injected (CTR) and NMDA-damaged (NMDA) retinae of GFAP-Cre/R26Y mice sacrificed 3wpi and immunostained for YFP (green), TUNEL (red) and CALR (magenta). Yellow arrows indicate $YFP^+/TUNEL^-$ cells expressing CALR, while red arrows indicate apoptotic $TUNEL^+$ cells (n = 3). Scale bar: 25 μm. (c) Quantification of $TUNEL^+$ apoptotic cells flat mounts from GFAP-Cre/R26Y mice belonging to the various treatment groups (CTR PBS, NMDA, NMDA + SDF1, NMDA + AMD3100), 1wpi and 3wpi. Values show the percentages of $TUNEL^+$ cells relative to the total $DAPI^+$ cells. Data are represented as mean ± S.E.M. ($n \geq 3$). Statistical analysis is based on unpaired Student's T-test ($p < 0.0001^{****}$) for samples 1wpi, and on One-way Anova ($p < 0.0001^{****}$) followed by Turkey's multiple comparisons test (significance indicated in the figure) for samples 3 wpi. (d) Quantification of $TUNEL^+$ apoptotic cells in flat mounts from GFAP-Cre/R26Y mice belonging to the four treatment groups (CTR PBS,

NMDA, NMDA + SDF1, NMDA + AMD3100), 3wpi. Values show the percentages of $TUNEL^+$ cells relative to the total $YFP^+/CALR^+$ cells. Data are represented as mean ± S.E.M. (n = 3). Statistical analysis is based on One-way Anova ($p = 0.0137^*$) followed by Turkey's multiple coomparisons test (significance indicated in the figure).

Figure S4. Macrophages infiltration in NMDA-damaged retinae. (a) Percentage of MAC-1^+ cells analyzed by FACS in damaged retinas from wild type mice at different time points (24hpi, 4dpi, 3wpi) after treatment (PBS, NMDA, NMDA + SDF1). Values represent means ± S.E.M. (n ≥ 3). Statistical analysis is based on Two-way Anova ($p = 0.5789^{ns}$) followed by Turkey's multiple comparisons test (significance indicated in the figure). (b) Representative FACS profiles of retinae from wild type mice sacrificed 24hpi and belonging to the different treatment groups (PBS, NMDA, NMDA + SDF1). Total retinal cells were stained for MAC-1 macrophage marker. Cells from peripheral blood (PB) and cells from unstained retinae (UNSTAINED) are also included in the analysis, as positive and negative controls respectively. $DAPI^+$ dead cells were excluded from the analysis. (c) Representative images of retinal flat mounts from GFAP-Cre/R26Y mice sacrificed 3wpi and belonging to the different treatment groups (CTR PBS, NMDA, NMDA + SDF1). Samples were stained for YFP (green), CALR (red) and MAC-1 (magenta). Yellow arrows indicate YFP^+ cells positive for CALR, whereas magenta arrows indicate MAC-1^+ cells (n = 3). Higher magnification fields are shown in the white squares. Scale bar: 25 μm.

Figure S5. The SDF1/CXCR4 axis regulates damage-dependent recruitment of bone marrow cells (BMCs), which can then fuse with retinal cells. (a) Representative FACS plots showing recruitment of RFP^+ BMCs into undamaged (CTR PBS) and damaged (NMDA) retinae of chimeric $R26Y/BM^{CRE\text{-}RFP}$ mice, 24hpi and 4dpi. Gating on total living retinal cells

was performed. (b) Representative FACS plots showing recruitment of RFP^+ BMCs, 24 hpi, in chimeric R26Y/$BM^{CRE\text{-}RFP}$ mice belonging to the different treatment groups (NMDA, NMDA + SDF1 and NMDA + AMD3100). $DAPI^+$ dead cells were excluded from the analysis. (c) Representative FACS plots showing fused hybrids (RFP^+/YFP^+) detected by FACS analysis in undamaged (CTR PBS) and damaged (NMDA) retinae of chimeric R26Y/$BM^{CRE\text{-}RFP}$ mice, 24hpi and 4dpi. YFP^+ hybrids are gated on recruited RFP^+ BMCs. $DAPI^+$ dead cells were excluded from the analysis. (d) Representative FACS plots showing the percentage of RFP^+ cells in the reconstituted total BM harvested from chimeric R26Y/$BM^{CRE\text{-}RFP}$ mice six weeks after sub-lethal irradiation and BM replacement. BM analysis from a wild type mouse was performed as a control (CTR). (e) Chimerism in R26Y/$BM^{CRE\text{-}RFP}$ mice, calculated as percentage of RFP^+ cells in the total BM (n = 15). Analysis by FACS was performed 6 weeks after the sub-lethal irradiation and BM replacement. Cells of total BM from wild type mice were used as negative controls. Statistical analyses are based on unpaired Student's T-test ($p < 0.0001^{****}$).

Figure S6. Bone marrow cells recruited into NMDA-damaged retinae preferentially fuse with Müller glia cells. (a) Representative images of retinal flat mounts from undamaged (CTR) and damaged (NMDA) R26Y/$BM^{CRE\text{-}RFP}$ chimeric mice sacrificed 24hpi (n = 3). Retinae were stained for YFP (green), RFP (red) and CRALBP (magenta). Zoomed images of the areas included in the white boxes are shown in the upper-right corners. Scale bar: 50 μm. (b) Percentage of $YFP^+/CRALBP^+$ hybrids relative to the total YFP^+ cells in retinal flat mounts of R26Y/$BM^{CRE\text{-}RFP}$ chimeric mice, 24hpi (n = 3). Statistical analyses are based on unpaired Student's T-test ($p < 0.0001^{****}$). (c) Representative immunostainings of YFP^+ hybrids (green) in sections of damaged R26Y/$BM^{CRE\text{-}RFP}$ retinae, 24hpi. Co-staining with various retinal markers is shown in red: REC (photoreceptors), PKC (bipolar neurons), CALR (ganglion and amacrine

cells) CALB (horizontal cells) (onl = outer nuclear layer, inl = inner nuclear layer, gc = ganglion cells layer). Nuclei were counterstained with DAPI. Red arrows indicate cells positive for specific neuronal markers, whereas yellow arrows indicate YFP^+ hybrids. Higher magnification images (from the areas enclosed by the white boxes) are shown in the left panels. Scale bar: 20 μm. (d) Schematic representation of the experimental plan. We used Calr-Cre/R26Y/BM^{RFP} chimeric mice, generated by replacing the BM of Calr-Cre/R26Y mice with the BM of CAG-RFP donor mice. In Calr-Cre/R26Y mice, ubiquitous expression of YFP is impeded by the presence of a floxed-STOP codon, which can be excised by Cre recombinase. Expression of Cre recombinase is driven by the ganglion and amacrine-specific calretinin promoter. As a consequence, the YFP reporter allows to trace ganglion and amacrine neurons. Additionally, YFP^+/RFP^+ double positive cells will result from fusion between YFP^+ ganglion/amacrine cells and RFP^+ transplanted BMCs. We injected NMDA in the right eyes of Calr-Cre/R26Y/BM^{RFP} chimeric mice. Left eyes were injected with PBS, as a control. Mice were sacrificed 24 hpi and 1 wpi for immunostaining and FACS analysis. (e) Representative FACS plots showing fusion events (RFP^+/YFP^+ hybrids) in chimeric Calr-Cre/R26Y/BM^{RFP} mice, in both undamaged (CTR PBS) and damaged (NMDA) retinae, 24 hpi. (f) Percentage of RFP^+ BMCs relative to total retinal cells in PBS- (CTR PBS) and NMDA-treated Calr-Cre/R26Y/BM^{RFP} chimeric mice, 24hpi. Values represent means ± S.E.M. (n = 3). Statistical analysis was based on unpaired Student's T-test ($p < 0.0001^{****}$). (g) Percentage of YFP^+/RFP^+ hybrids relative to total retinal cells in undamaged (CTR PBS) and damaged (NMDA) retinae of Calr-Cre/R26Y/BM^{RFP} chimeric mice, 24hpi. Values represent means ± S.E.M. (n = 3). Statistical analyses are based on unpaired Student's T-test ($p = 0.1284^{ns}$).

Figure S7. YFP^+ hybrids re-enter the cell cycle and do not undergo apoptosis following NMDA-damage. (a) Representative images of flat mounted retinas from undamaged (CTR) and damaged (NMDA) GFAP-Cre/BM^{R26Y} chimeric mice sacrificed 24hpi (n = 3). Retinae

were stained for YFP (green) and CRALBP (magenta). Yellow arrows indicate YFP^+ hybrids that are also positive for CRALBP expression, whereas green arrows indicate YFP^+ hybrids that are CRALBP-negative. Zoomed images of the areas included in the white boxes are shown in the upper-left corners. Scale bar: 20 μm. (b) Percentages of $YFP^+/CRALBP^+$ hybrids relative to the total number of YFP^+ hybrids counted in random fields of flat mounts from 3 different, NMDA-damaged GFAP-Cre/BM^{R26Y} eyes, 24 hpi (n = 3). Statistical analyses are based on unpaired Student's T-test ($p < 0.0001^{****}$). (c) Representative immunofluorescence images of retinal flat mounts from undamaged (CTR) and damaged (NMDA) GFAP-Cre/BM^{R26Y} chimeric mice sacrificed 24hpi. Retinae were stained for YFP (green) and MAC-1 (red). Yellow arrows indicate co-localization between the two markers. Green arrows point at YFP^+ hybrids that are negative for MAC-1. Scale bar: 50 μm. (d) Representative images of retinal flat mounts from undamaged (CTR) and damaged (NMDA) GFAP-Cre/BM^{R26Y} chimeric mice**,** sacrificed 24hpi (n = 3). Retinae were stained for YFP (green) and TUNEL (red). Scale bar: 20 μm. (e) Percentage of YFP^+ hybrids relative to the total number of $DAPI^+$ cells counted in retinal sections of undamaged (CTR) and damaged (NMDA) GFAP-Cre/BM^{R26Y} chimeric mice sacrificed 24hpi (n = 3). Apoptotic hybrids are also shown; they were quantified as percentage of $TUNEL^+$ cells over the total YFP^+ hybrids (gray bar). Statistical analysis is based on Two-way Anova ($p < 0.0001^{****}$). (f) Representative immunostaining images of retinal sections from damaged retinae (NMDA) of chimeric GFAP-Cre/BMR26Y mice, 24hpi. Co-localization between YFP (green) and phH3 (red) is indicated by yellow arrows. Nuclei were counterstained with DAPI (blue). Zoomed images of the areas included in the white boxes are shown in the upper-left corners Scale bar: 20 μm.

Figure S8. YFP$^+$ hybrids can differentiate into CALR$^+$ cells in the long term. (a) Quantification of the total number of CALR$^+$ ganglion-amacrine cells in retinal flat mounts from control (not irradiated and not transplanted GFAP-Cre mice) and irradiated and transplanted GFAP-Cre/BM^{R26Y} chimeric mice (n = 3). Statistical analysis is based on unpaired Student's T-test ($p = 0.3031^{ns}$). (b) Representative immunostaining of retinal flat mounts from undamaged (CTR) and damaged (NMDA) GFAP-Cre/BM^{R26Y} mice, 3wpi. Retinae were stained for YFP (green), CALR (red) and GS (magenta). Nuclei were counterstained with DAPI. Yellow arrows indicate co-localization of YFP and CALR, whereas magenta arrows indicate co-localization of YFP and GS. Red arrows point at YFP$^+$/CALR$^+$/GS$^+$ cells. Scale bar: 10 μm. (c) Representative images of retinal flat mounts from undamaged (CTR) and damaged (NMDA GFAP-Cre/BM^{R26Y} chimeric mice, 3wpi. Retinae were stained for YFP (green) and MAC-1 (red). Green arrows indicate YFP$^+$ cells that are negative for MAC-1 expression. Zoomed images of the areas included in the white boxes are shown in the lower-right corners. Scale bar: 25 μm.

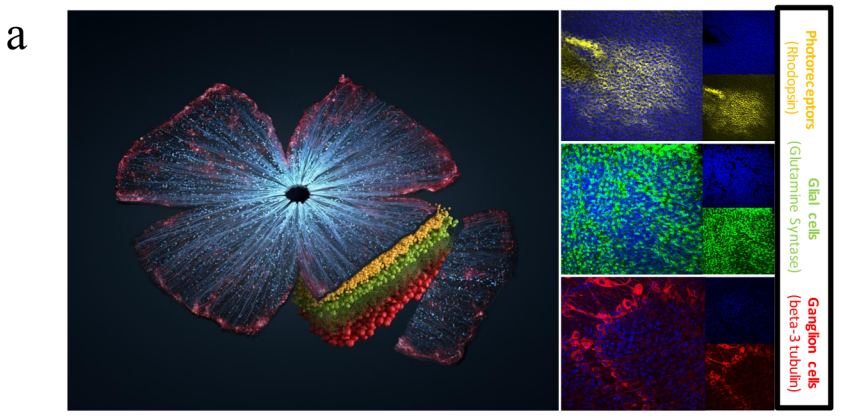

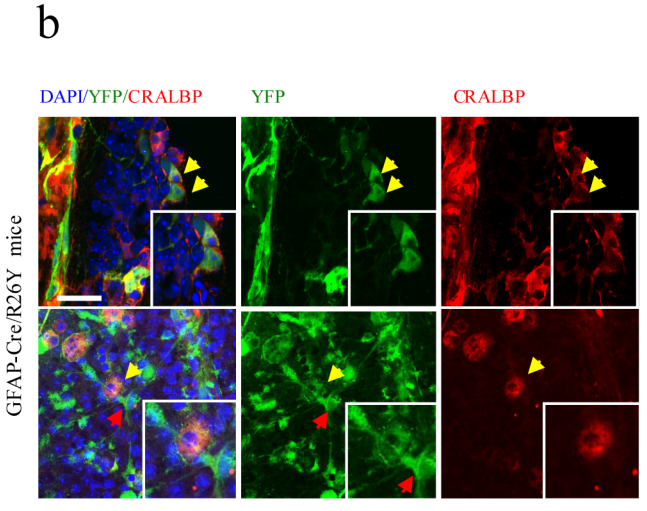

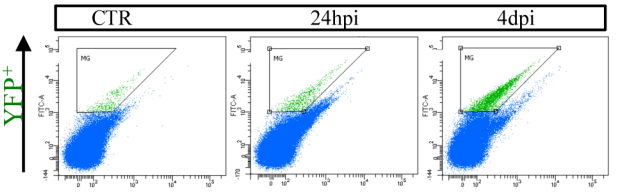

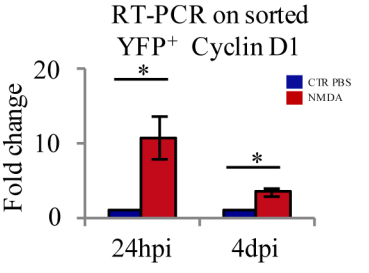

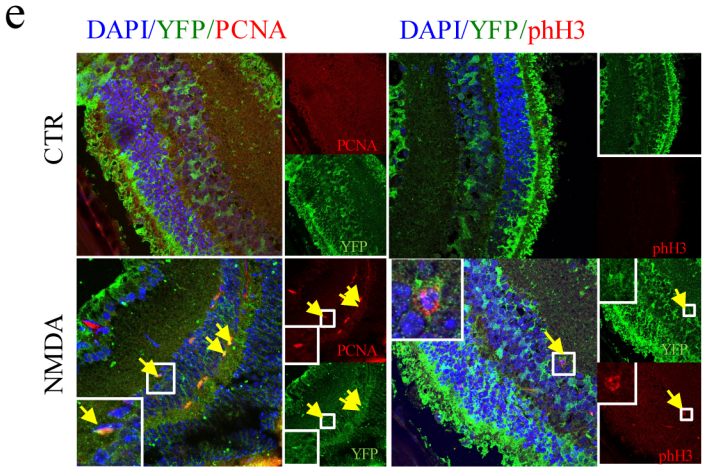

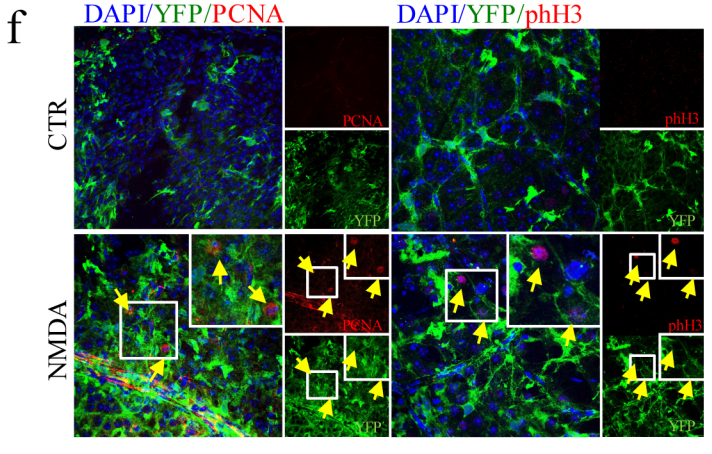

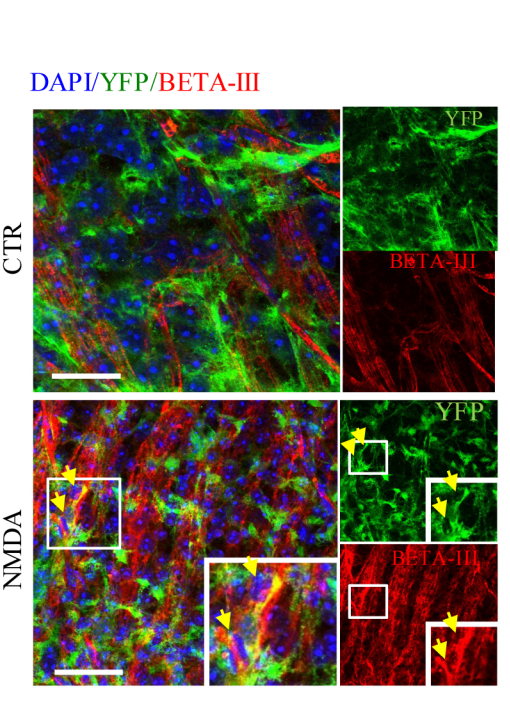

Pesaresi et al. Figure S1

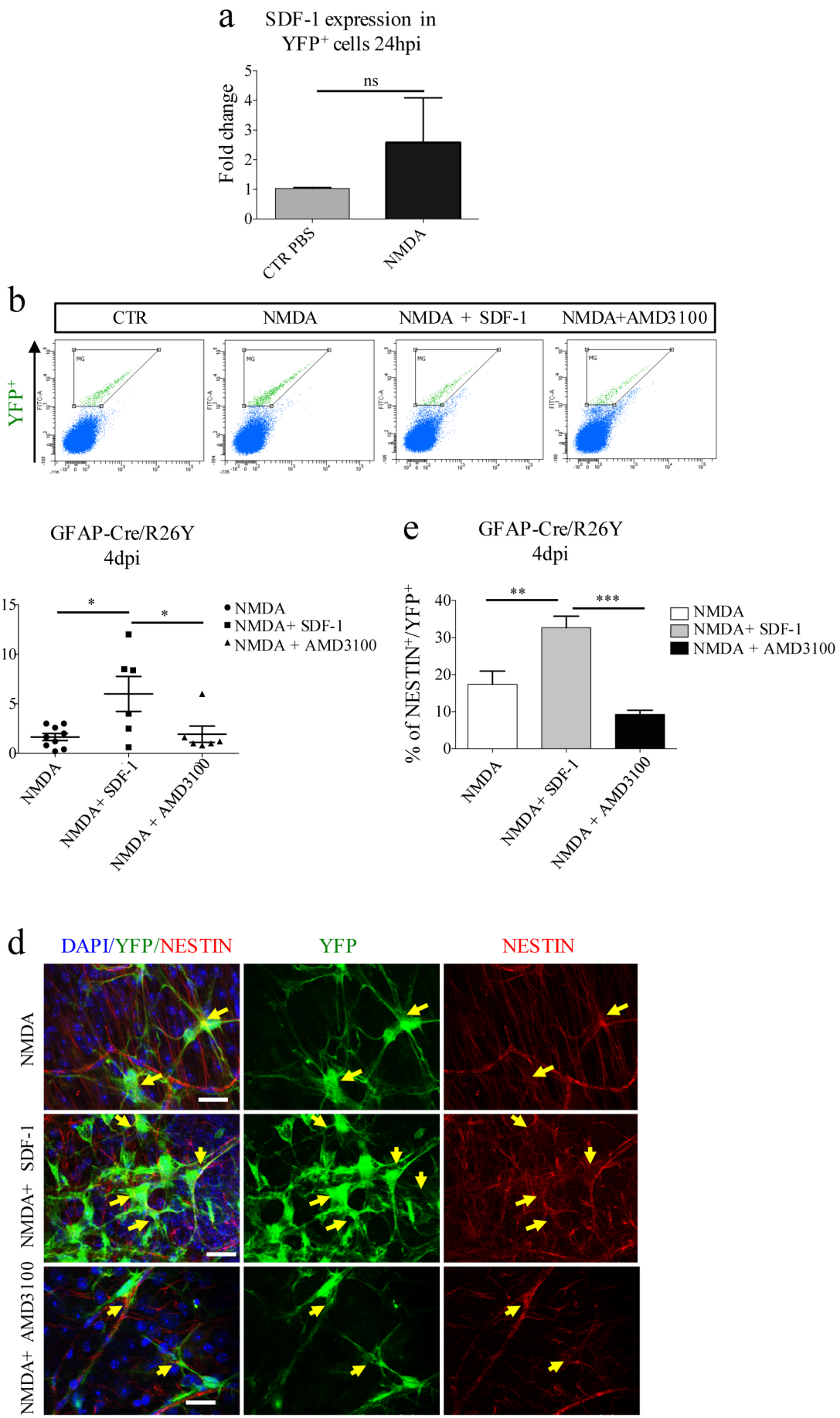

Pesaresi et al. Figure S2

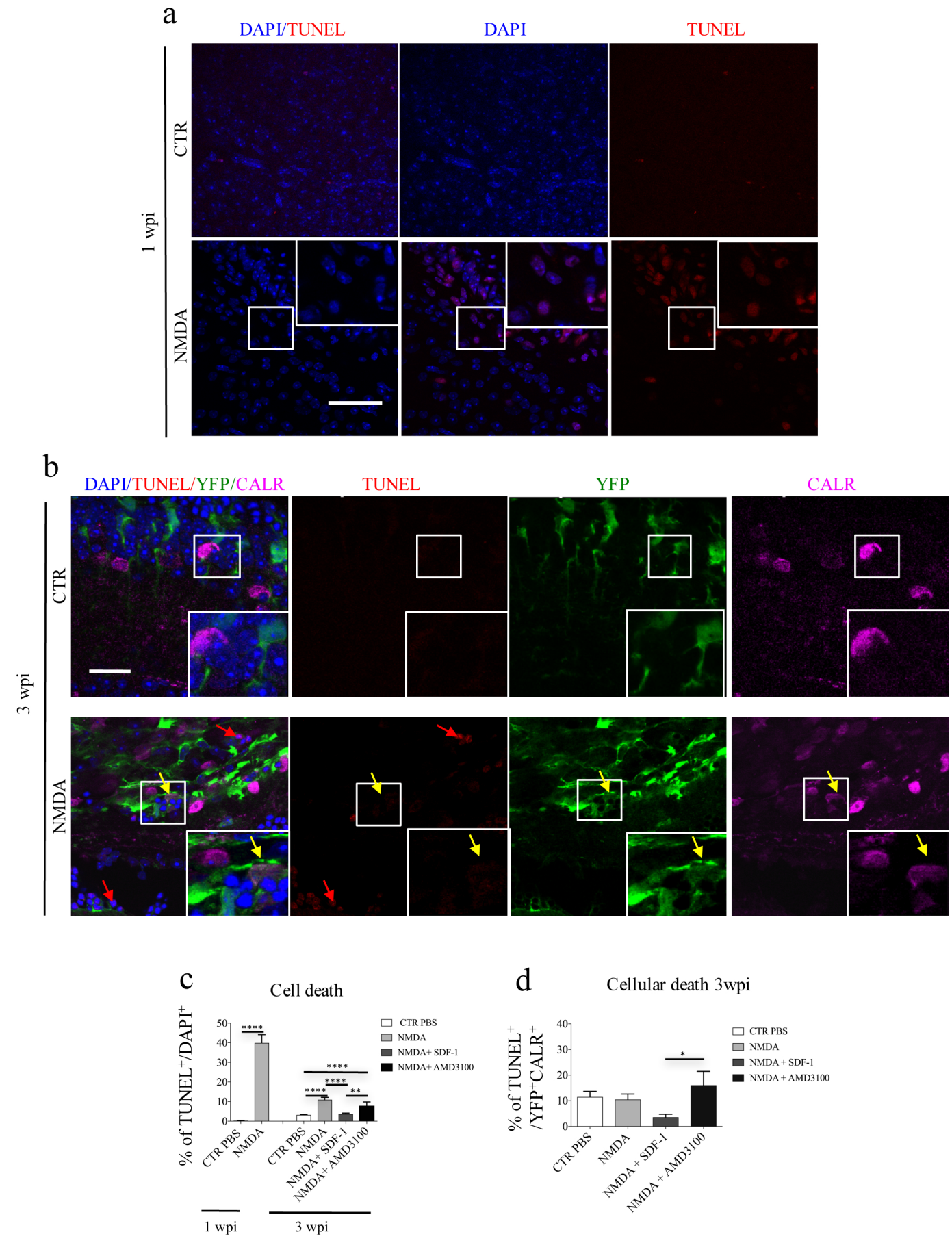

Pesaresi et al. Figure S3

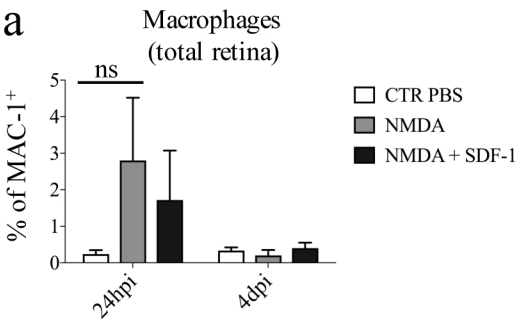

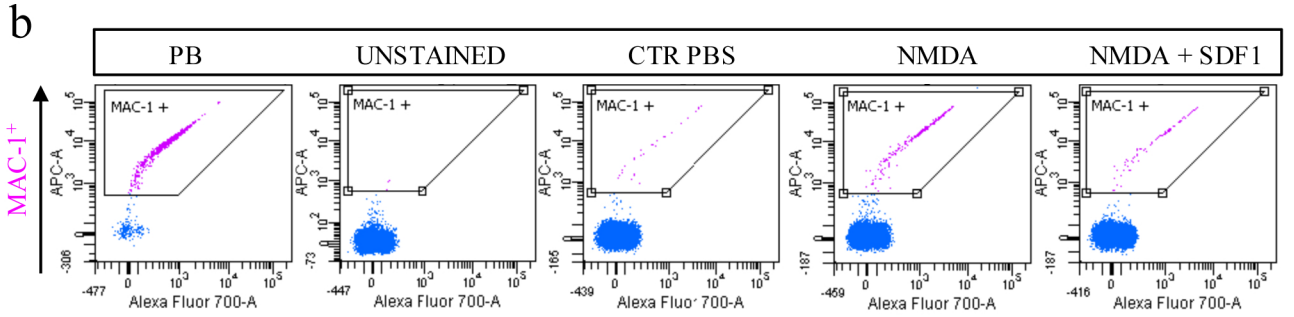

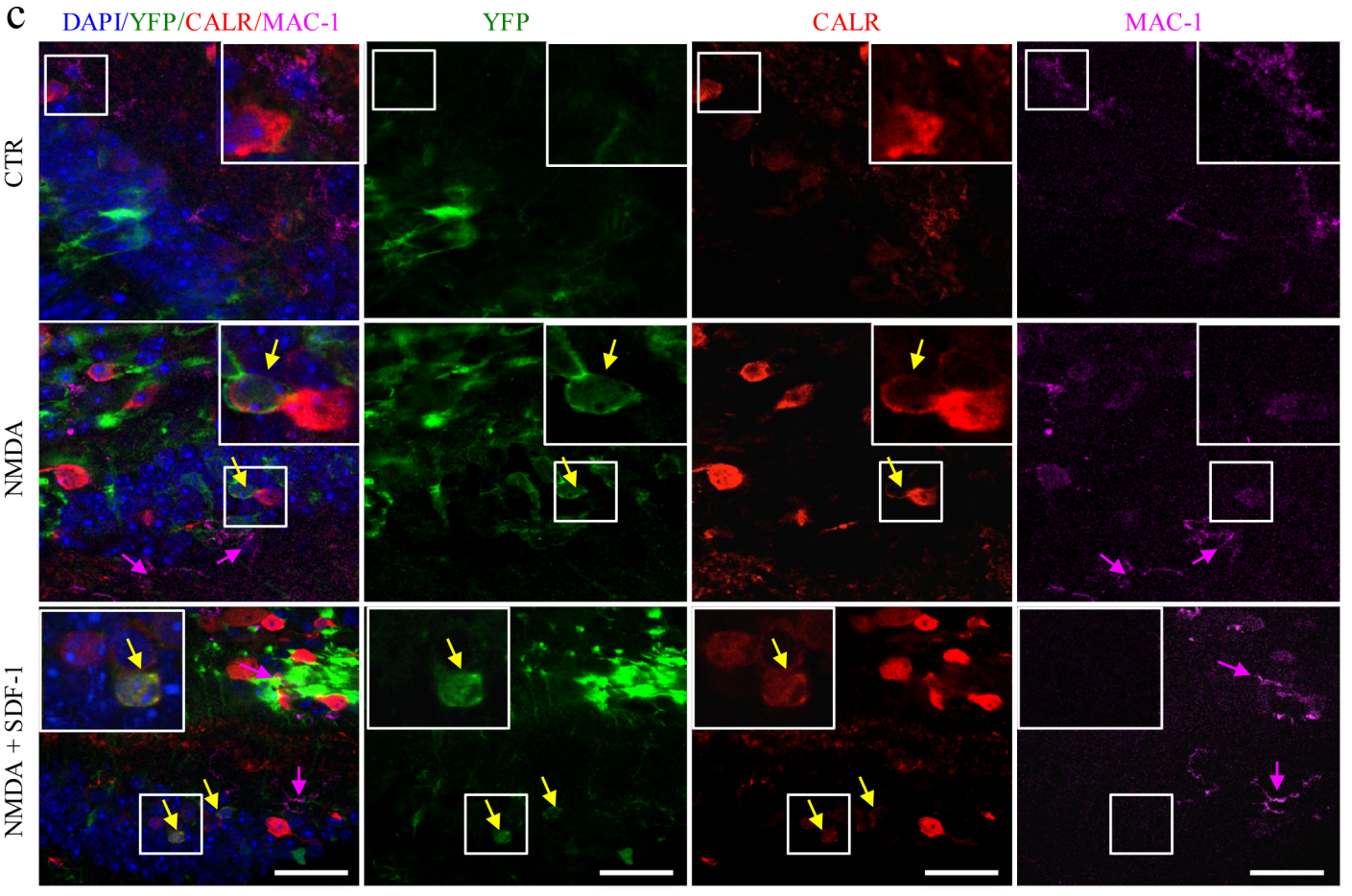

Pesaresi et al. Figure S4

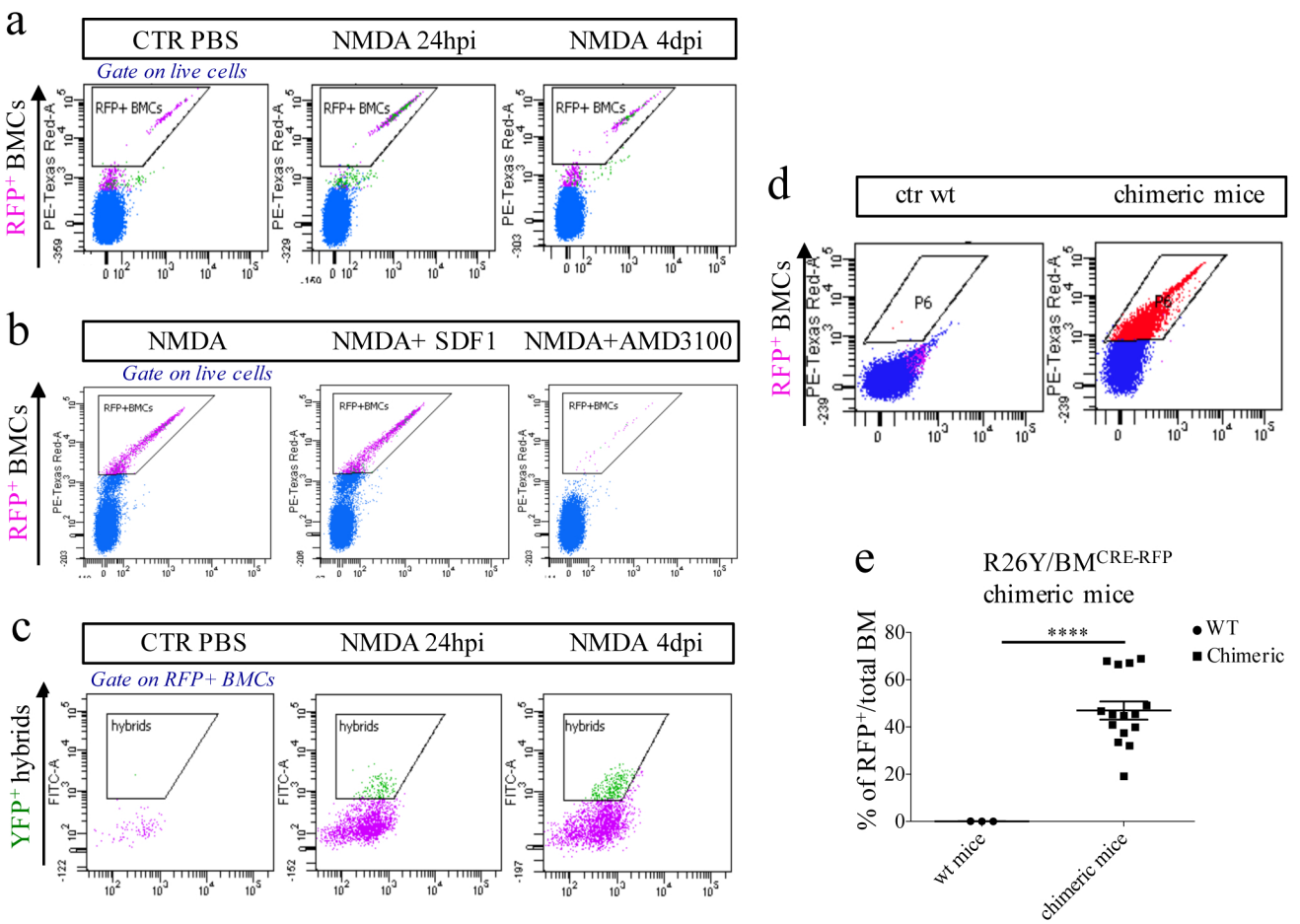

Pesaresi et al. Figure S5

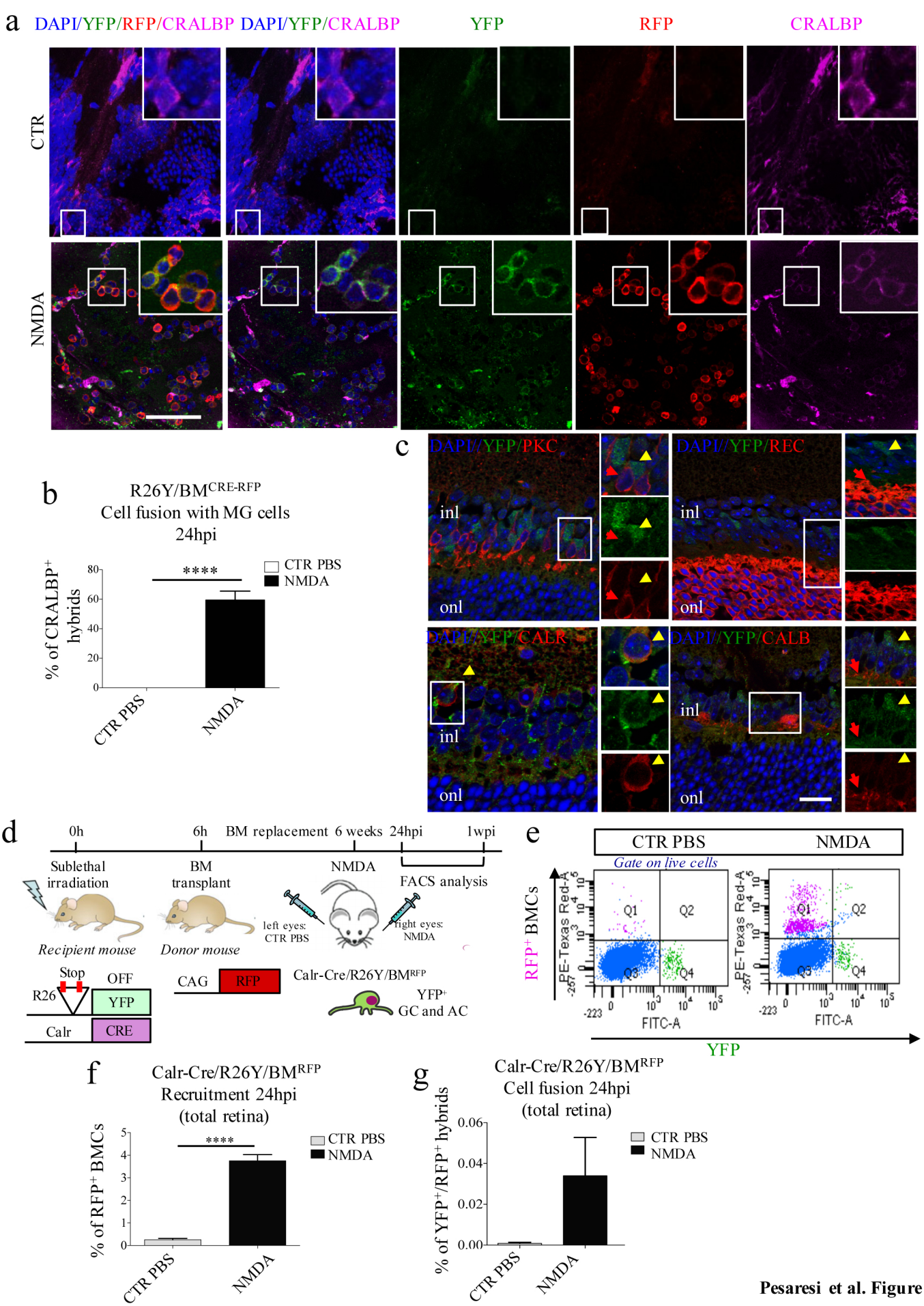

Pesaresi et al. Figure S6

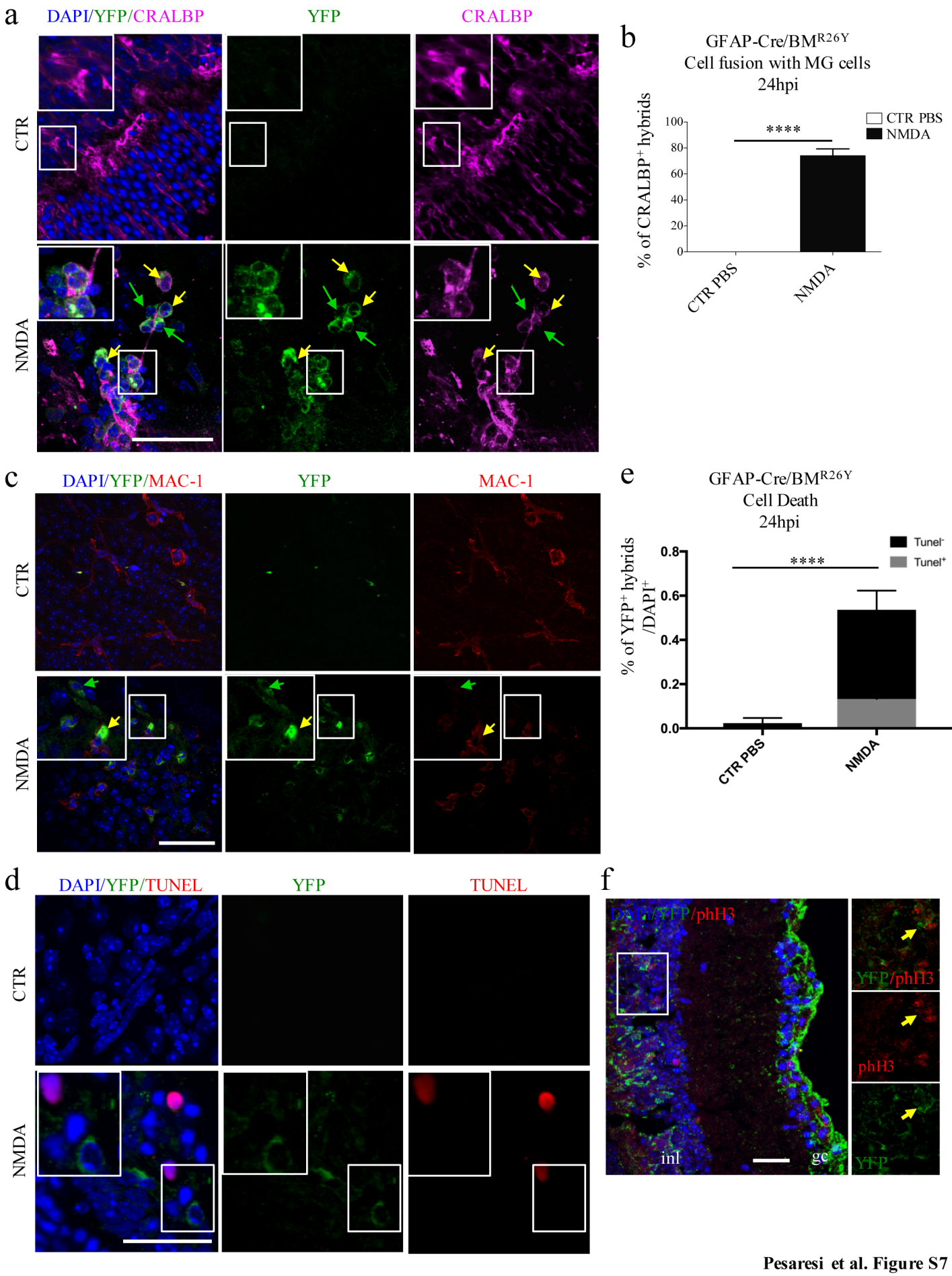

Pesaresi et al. Figure S7

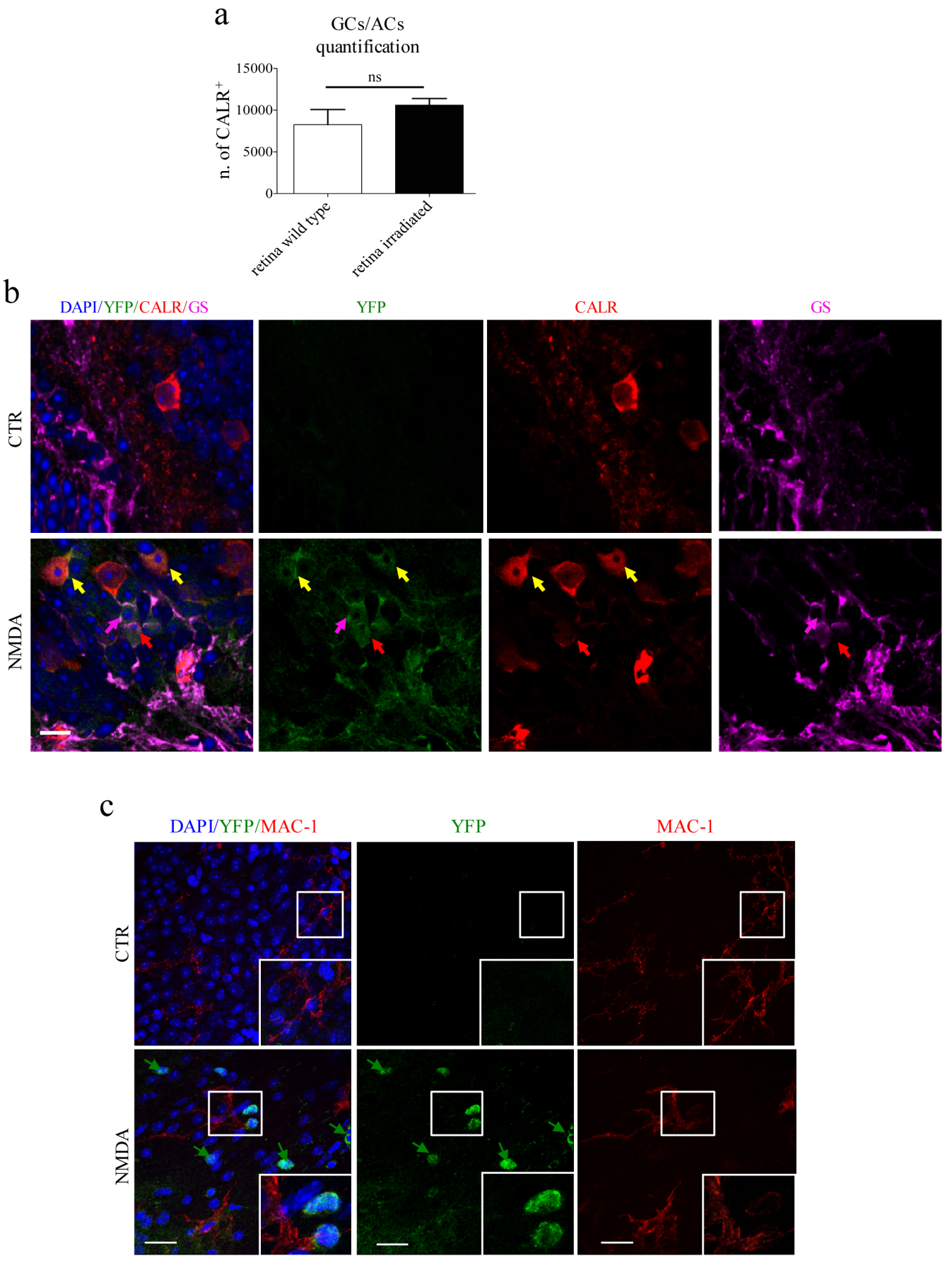

Pesaresi et al. Figure S8